FORCED CONVECTION OVER A THREE-DIMENSIONAL HORIZONTAL BACKWARD FACING STEP

By

J.G. Barbosa Saldana and **N.K. Anand**

Department of Mechanical Engineering

and

V. Sarin

Department of Computer Science

Texas A&M University
College Station, Texas 77843

A Paper submitted for publication in

International Journal of Computational Engineering Science

Submitted July 2004

Corresponding Author: N.K. Anand (nkanand@tamu.edu)

Abstract

Forced convective flow over a 3-D Backward-Facing step is studied numerically. The momentum and energy equations were discretized by means of a finite volume technique. The SIMPLE algorithm scheme was used to link the pressure and velocity fields in the entire domain and a line-by-line scheme was used in each plane to compute the velocity, pressure, and temperature field distributions. The code was validated by comparing numerical predictions with experimental data for flow over a 3-D backward facing step that is available in the literature.

Flow of air (Pr=0.70) over a three-dimensional horizontal backward-facing step geometry with an aspect ratio AR=8 and an expansion ratio ER=2 was considered. The stepped wall downstream of the expansion was heated by subjecting it to a constant heat flux (q_w=50 Wm^{-2}) and the other walls were considered as insulated. The inlet flow was taken to be hydro-dynamically fully developed with a uniform temperature profile. Locations where the streamwise velocity and the spanwise velocity components are zero for the nearest plane adjacent to the stepped wall were plotted for different Reynolds numbers. Distributions for local and average Nusselt number for the stepped wall, and graphical representations for u, v, and w velocities components obtained in these simulations are presented in the paper.

Introduction

Even though the separated and reattached flow is present in several industrial applications, this phenomenon is not completely understood due to the complex flow structures. Separation and reattachment of flow is present in heat transfer applications such as cooling of electronic equipment, cooling of nuclear reactors, cooling of turbine blades, flow in combustion chambers, flow through channels whose area is suddenly augmented like wide-angle diffusers, and flow in valves (Nie and Armali, 2002 and Iwai et. al., 2000).

Studies on separated and reattached flow have been conducted extensively and the flow over a backward facing step has become the central point for both experimental and numerical investigations. Although it has a very simple geometry, the flow over the backward facing step presents the most important flow structures associated with the separation and reattached flow. The flow in a backward facing step channel is featured as having a shear layer separation, a region of recirculation flow just behind the step, and under some conditions, a region of recirculation flow attached to the roof of the channel (Chiang et. al., 1997).

The first efforts for studying the separation and reattachment flow over a backward facing step were made in late 1950's. Interest in studying and understanding the three-dimensional flow structures associated with separation and reattachment phenomena in this geometry increased in the last two decades with the development of sophisticated flow visualization techniques and recent developments in computer hardware.

Shih and Ho (1994) published experimental results for flow of water over a backward facing step with aspect ratio AR=3. Similar measurements for air flow over a backward facing step in a duct with aspect ratio AR=8 and expansion ratio ER=2.02 were published by Armaly et. al. (2003). Both publications concluded that the recirculation zone is distorted across the spanwise direction due to strong three-dimensionality of the flow behind the back step.

The aspect of numerical simulations of the backward facing step has been considered by several authors not only for the fluid flow problem but also for the heat transfer problem. Iwai et. al.

(2000) studied numerically the effect of aspect ratio on the development of flow over a three-dimensional backward facing step and the forced convection effects along top and bottom walls when subjected to constant high temperature. They suggested that for AR>16 the phenomena can be simplified as two-dimensional. Forced convection due to a constant heat flux at the bottom and top walls for a duct with an aspect ratio AR=12 was studied numerically by Carrington and Pepper (2002) using a finite element technique.

A study of the three dimensional topology of the flow over a backward facing step was presented by Chiang et. al. (1997). Their objective was to get a deeper and realistic physical interpretation of the fluid flow behind the back step by utilizing a rigorous mathematical foundation to find characteristic points for flow separation and reattachment. This study revealed that the flow presents complex and highly three-dimensional structures.

Nie, Armaly, and collaborators numerically simulated the fluid and forced convective flow over a three-dimensional backward facing step (Nie and Armaly, 2002; Nie and Armaly, 2003; Armaly et. al., 2002; Armaly et. al., 2003). They suggested that for a three-dimensional flow, the reattachment on the stepped wall is distorted in the spanwise direction and that the wall shear stress is equal to zero only at one point on the bottom plane.

The information and data generated numerically and experimentally for studying flow over three-dimensional backward facing step is enormous through the years. In spite of a large body of data there was no a solid base for comparing the results and defining an accurate methodology for solving the problem, as well as identifying parametric values to describe the most important features of separation and reattachment flow. In this sense the present work adds to the numerical data for the benchmark problem of forced convective flow over a backward facing step and has significant tutorial value.

Model Description and Numerical Procedure

Forced convective flow over a three-dimensional backward facing step was numerically simulated via a finite volume discretization technique. The channel aspect ratio and expansion ratio were fixed in relation to the step height (s=0.01) as AR=8 and as ER=2, respectively. The

step length in the streamwise direction is *l*=2s and the channel length from the step to the channel exit is equal to 50 times the step height (L=50s). The geometry is shown in Fig. 1.

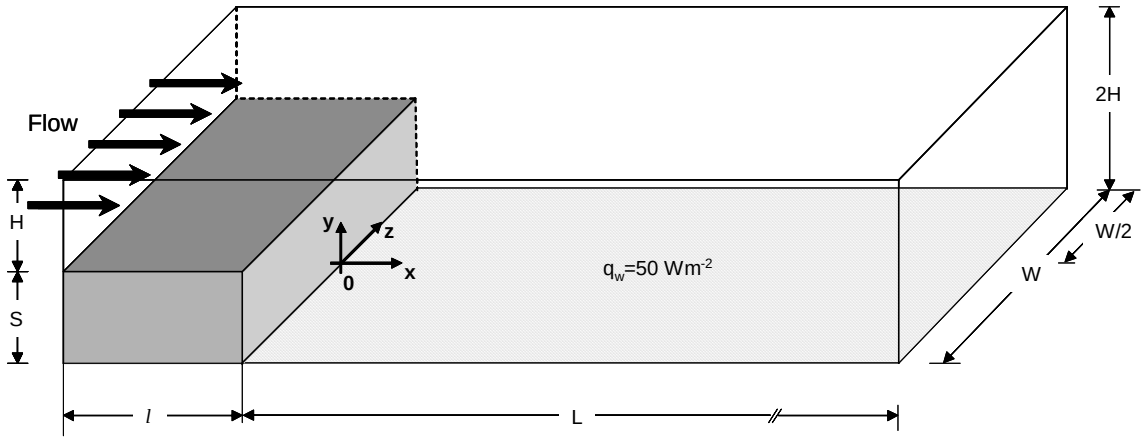

Fig. 1 Backward facing step.

When the fluid flow and heat transfer problem is considered to be steady state, the mass conservation, momentum, and energy equations governing the phenomena are reduced to the following forms; [Kakac and Yener, 1995]:

Continuity Equation:

$$\nabla \cdot \left(\rho V \right) = 0 \tag{1}$$

Momentum Equation:

$$V \cdot \nabla \left(\rho V \right) = -\nabla p + \nabla \cdot \left(\mu \nabla V \right) \tag{2}$$

Energy Equation:

$$V \cdot \nabla \left(\rho C p T \right) = \nabla \cdot \left(k \nabla T \right) \tag{3}$$

At the duct entrance the flow was treated as fully developed (Shah and London, 1978) and isothermal. No-slip condition was applied at the duct walls, including the step. The bottom wall of the channel ($0 \le x \le L$; $-W/2 \le z \le W/2$) was subjected to a constant heat flux (q_w=50 Wm^{-2}) and the rest of the walls were treated as adiabatic.

The physical properties of air in the numerical procedure were treated as constants and evaluated at the flow inlet temperature: T_0=293 ^oK, ρ =1.205 kg/m^3, μ =1.81x10^{-5} kg/m-s, Cp=1005 J/kg-^oK, k =0.0259 W/m-^oK.

A FORTRAN code was developed to numerically study the stated problem. A finite volume technique was used to discretize the momentum and energy equations inside the computational domain. The SIMPLE algorithm was used to link the pressure and velocity fields. Solution to the one-dimensional convection-diffusion equation at the control volume interfaces was represented by the power law (Patankar, 1980). Velocity nodes were located at staggered locations in each coordinate direction while pressure, temperature, and other scalar properties were evaluated at the main grid nodes.

To simulate the solid block inside the domain a very high diffusion coefficient for the momentum equations was chosen ($\mu=10^{50}$), and to solve the energy equation the thermal diffusion coefficient was set equal to an extremely low value ($k_s=10^{-50}$). At the solid-fluid interface the diffusion coefficients where evaluated by a weighted harmonic mean of the properties in neighboring control volumes (Patankar, 1980).

A combination of the line-by-line solver and the Tri-diagonal matrix algorithm was used for each plane in x-, y-, and z-coordinate directions to compute the velocity, pressure, and temperature inside the computational domain. Under-relaxation for the velocity components ($\alpha_u=\alpha_v=\alpha_w=0.4$) and pressure ($\alpha_p=0.4$) were imposed. Convergence was declared when the normalized residuals for the velocity components and pressure were less than 10^{-8}. For the temperature, the convergence criteria requires that the maximum relative change in the temperature be less than 10^{-6}.

A non-uniform grid size was considered for the problem. At the solid walls the grid was very fine and it was deployed by using a geometric expansion factor. The grid independence study was conducted by using several grid densities for Re=512. The location at the central plane in the spanwise direction (z=0) where the streamwise component of the wall shear stress is zero was monitored to declare grid independence. The numerical results were compared against the measurements published by Armaly, et. al. (2003) and the results are summarized in Table 1.

Table 1. Grid independence study

Experimental location of zero streamwise shear stress component. (Armaly, et.al., 2003): $(x/s)_{experimental}=10.58$

Grid size x-y-z	Expansion factors e_x-e_y-e_z	x/s (present)	% difference $\left[\frac{\left(\frac{x}{s}\right)_{present}-\left(\frac{x}{s}\right)_{experimental}}{\left(\frac{x}{s}\right)_{present}}\right]x100$
180-40-80	1.025-1.35-1.08	10.967	3.46
180-40-60	1.025-1.35-1.08	10.964	3.51
160-40-80	1.025-1.35-1.08	11.02	3.99
160-40-60	1.025-1.35-1.08	11.01	3.9
140-40-60	1.025-1.35-1.08	10.771	1.76

Based on the results shown in Table 1, the grid 140x40x60 with expansion factors 1.025, 1.35, and 1.08 in x, y, and z directions, respectively, was chosen to make parametric runs.

Once grid independence was established, the second step was to validate the numerical code. The validation tests were conducted for Re=343 and Re=512. The results for the so called x_u-line, as well as results for the u-velocity component at specific planes were compared against the results published by Armaly et. al. (2003) and plotted in Figs. 2 and 3. The x_u-line is a locus of points wherein the streamwise component of the velocities are zero. It is evident from Figs. 2 and 3 that the numerical predictions using the code agree very well with the experimental data of Armaly et. al. (2003), thus validating the code.

Numerical Results and Discussion

The numerical study presented in this work considers the convective air-flow over a backward facing step (Fig. 1) for four different Reynolds numbers. The Reynolds number is based on the bulk velocity at the duct entrance and twice the channel's step height. Solutions for Re=98.5, 200, 343, 400, and 512 are presented. The bottom wall of the channel is subjected to a constant heat flux (q_w=50Wm^{-2}).

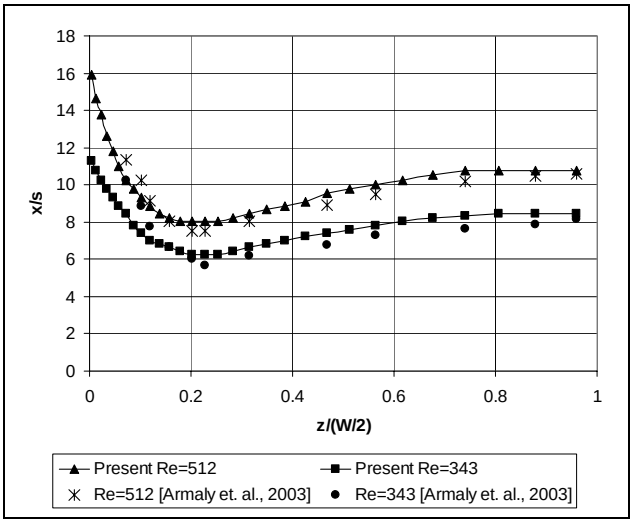

Fig. 2 x_u-line numerical validation.

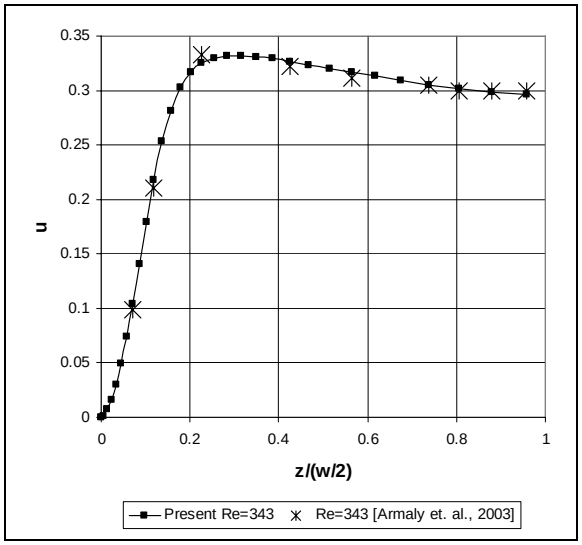

Fig. 3 Validation for u-velocity component at y/s=1 and x/s=5.

Due to the symmetry present in the backward facing step problem many numerical studies simulate half of the channel in the spanwise direction. However, this assumption was not used in this numerical study and the simulation was done for the full spanwise width in the z-direction. The coordinate origin was placed as shown in Fig. 1.

Figure 4 shows the x_u-line adjacent to the bottom wall for different Reynolds numbers.

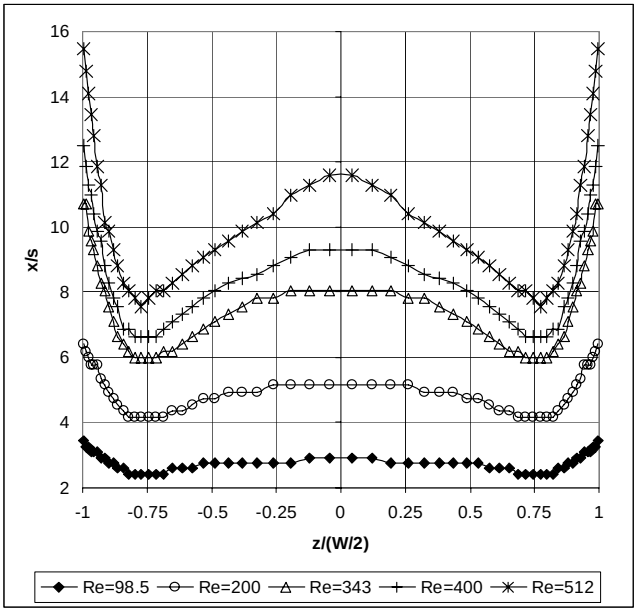

Fig. 4. x_u-line distributions adjacent to the bottom wall.

The x_u-line represents the points in the spanwise direction where the streamwise component of the wall shear stress is equal to zero. This line has a close relation with the edge of the primary recirculation zone behind the back step. Figure 4 shows that this line presents a symmetrical behavior with respect to the central plane in the spanwise direction (z direction). However, the line is not straight and has variations in the spanwise direction. The lowest value of x_u-line is located near the lateral walls approximately at $z/(W/2)=\pm 0.75$. The maximum value is in the vicinity of the lateral walls.

The distribution of the x_u-line is highly influenced by the Reynolds number. For high Reynolds number this line is pushed further downstream of the back step. The spanwise distribution for the x_u-line presents strong variations as the Reynolds number increases. In Fig. 4 this line is almost a straight line for Re=98.5, and has a shape similar to a big "W" for Re=512.

If the same concept for computing the x_u-line is used for the w-velocity component, the result is the x_w-line. Hence, the x_w-line represents the points adjacent to the bottom wall where the spanwise component of the wall shear stress is equal to zero. Figure 5 shows the x_u-line and the x_w-line at different Reynolds numbers.

The x_w-line has a parabolic profile that is symmetric with respect to the central plane in the z-direction. Similar to the x_u-line, the effect of Reynolds number on the x_w-line is to push the location further in the streamwise direction.

As can be seen in Fig. 5, the x_u-line and the x_w-line intersect a common point in the spanwise direction. According to the definitions for both lines this point should represent the location where the shear stress along the bottom wall is zero. This point is located near the side walls, almost coinciding with the minimum value of the x_u-line. The location of this point in the spanwise direction seems to be constant and independent of Reynolds number. However, the location in the streamwise direction moves downstream as the Reynolds number increases. Table 2 summarizes the position of this point at different Reynolds numbers.

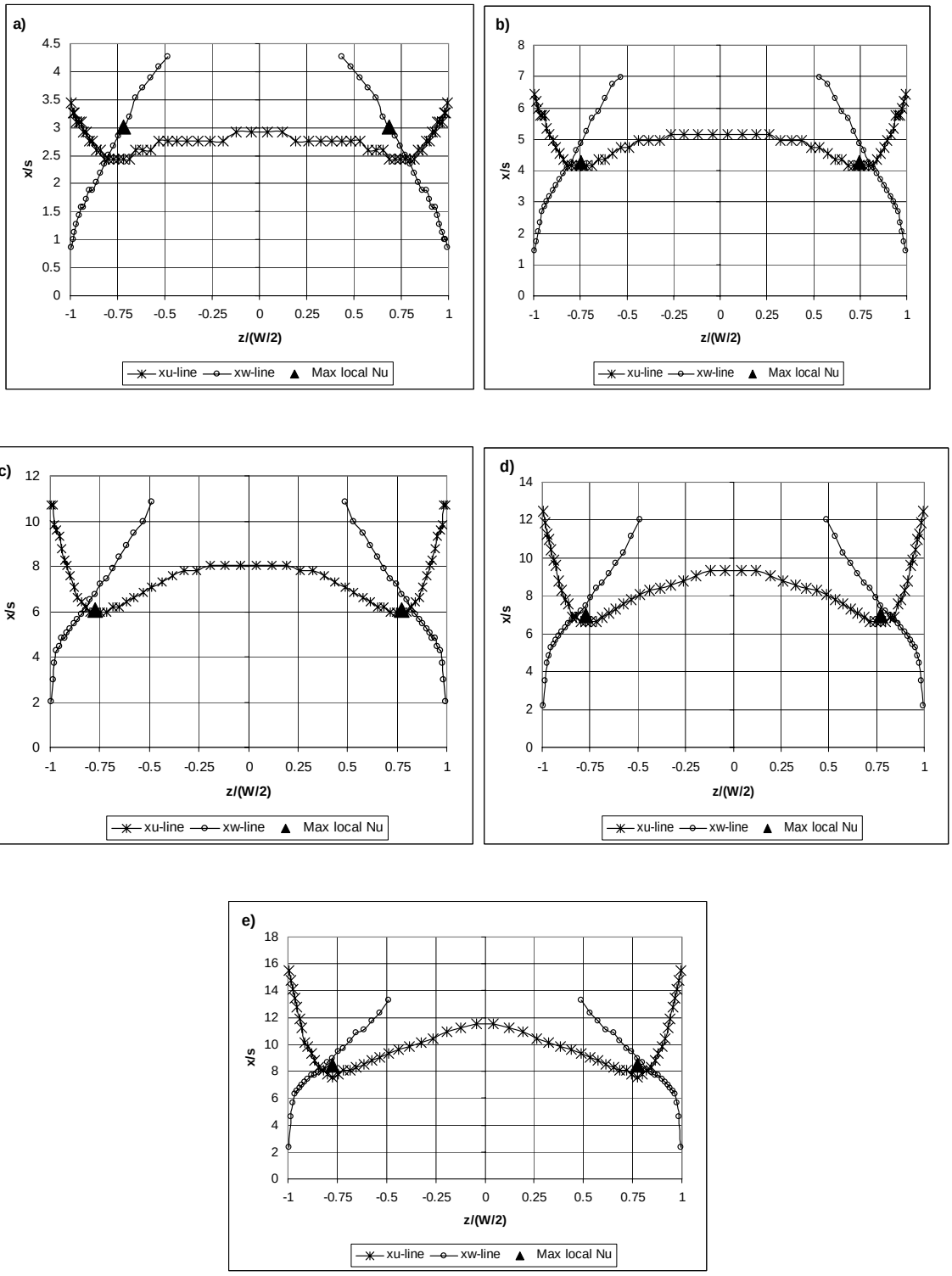

Fig. 5 x_u-line and x_w-line in the spanwise direction
a) Re=98.5, b) Re=200, c) Re=343, d) Re=400, and e) Re=512.

Table 2. Locations for τ=0 along the bottom wall		
Re	x/s	z/(W/2)
98.5	2.42	±0.80
200	4.17	±0.82
343	6.10	±0.82
400	6.86	±0.82
512	8.10	±0.82

The streamwise shear stress component averaged in the z direction for different Reynolds number is plotted in Fig. 6.

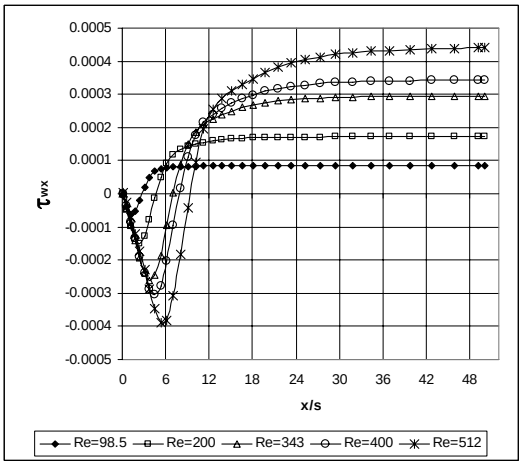

Fig. 6 Streamwise shear stress component averaged in the spanwise direction.

In general, higher values of shear stress are associated with higher Reynolds numbers. In Fig. 6, it can be seen that a region of negative values for the streamwise shear stress component is located just downstream of the step (x/s=0). This zone has a close relation with the primary recirculation zone. The point, where the value is zero, could be interpreted as "*the average reattachment point*". This point is shifted further downstream as Reynolds is increased. The locations, where τ_{wx} is equal to zero, are summarized in Table 3. At the channel exit the flow behaves like a fully developed flow.

Table 3. Locations of zero average streamwise shear stress component				
Re=98.5	Re=200	Re=343	Re=400	Re=512
x/s=2.77	x/s=4.55	x/s=6.20	x/s=7.09	x/s=9.06

The spanwise average Nusselt number distribution for flow over the backward facing step is presented in Fig.7. The Nusselt number distribution starts with a low value at the backstep, increases until it reaches a peak value, and then monotonically decreases towards the channel exit. Thermally fully developed condition was not reached for any of the cases considered in this study. The results show a similar tendency for all the Nusselt number distributions; higher values were found for higher Reynolds numbers.

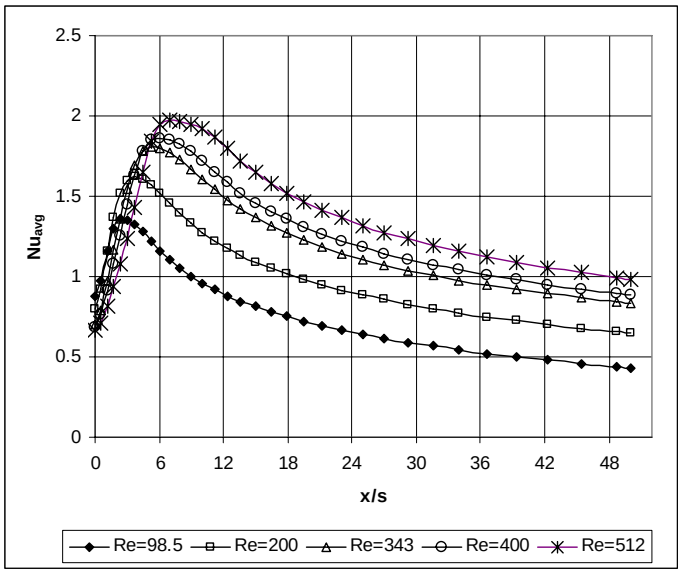

Fig. 7 Spanwise average Nusselt number distributions at different Reynolds numbers.

Figure 7 shows that the peak of the spanwise average Nusselt number distribution is moved further downstream of the backstep as the Reynolds number is increased. The peak values and their locations for each case are summarized in Table 4.

Table 4. Locations of the peak streamwise average Nusselt number distribution				
Re=98.5	Re=200	Re=343	Re=400	Re=512
Nu_{avg}=1.36	Nu_{avg}=1.62	Nu_{avg}=1.80	Nu_{avg}=1.86	Nu_{avg}=1.97
x/s=2.35	x/s=3.71	x/s=5.25	x/s=6.09	x/s=6.98

As can be observed from Tables 3 and 4, the location of the maximum spanwise average Nusselt number occurs upstream of the zero spanwise average streamwise shear stress. In other words, the maximum spanwise average Nusselt number occurs inside the primary recirculation zone adjacent to the backstep.

The streamwise and spanwise coordinates, where the local Nusselt number is a maximum, are plotted in Fig. 5 and are summarized in Table 5.

Table 5. Streamwise and spanwise coordinates of the maximum local Nussel number			
Re	x/s	z/(W/2)	Nu
98.5	3.01	±0.72	1.48
200	4.08	±0.77	1.88
343	6.09	±0.77	2.17
400	6.98	±0.77	2.26
512	8.42	±0.77	2.45

The maximum local Nusselt number is located near the side walls and its location is very close to the point where the shear stress along the bottom wall is equal to zero. This is evident from the results in Tables 2 and 5. The position of the maximum local Nusselt number lies approximately on the x_u-line for all the cases simulated in this study except for Re=98.5, as can be seen in Fig. 5

Figure 8 presents u-component velocity profiles at the central plane in the spanwise direction (z/W=0) for different constant x-planes.

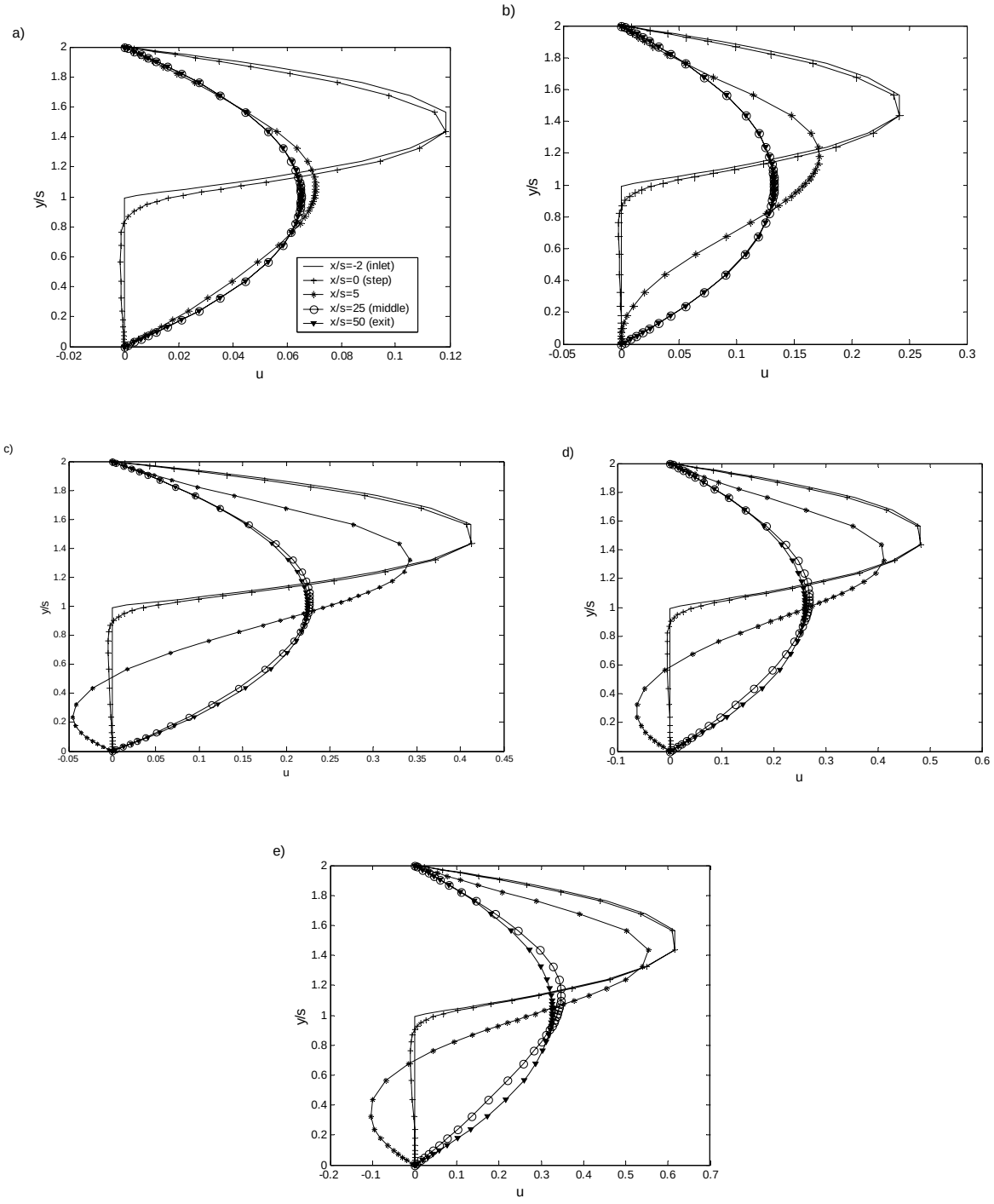

Fig. 8 U-velocitiy component at different x planes for the spanwise's central plane (z/W=0)
a) Re=98.5, b) Re=200, c) Re=343, d) Re=400, and e) Re=512.

At the inlet the flow is considered to be fully developed. At the plane x/s=5 the recirculation zone is completely identified for Re≥343 by the negative values in the u-velocity component. For Re=98.5 there is no recirculation zone in this x-plane and even the velocity profile in this plane

resembles a fully developed flow near the exit. For Re=200 in Fig. 8(b) a very small recirculation zone is located in the vicinity of the bottom wall (y/s=0) for x/s=5. Figures 8(c)-8(e) show a perfectly defined recirculation zone adjacent to the bottom wall. This zone becomes larger as the Reynolds number increases.

At the middle of the channel (x/s=25), the flow has passed the primary recirculation zone and is being redeveloped towards the channel exit. However, the conditions for fully developed flow at the channel exit are not achieved for all cases considered in this study, and small deviations in the velocity profile are present for Re≥343. The other two cases for Re=98.5 and Re=200 do achieve the conditions of fully developed flow at the channel exit. Symmetry with respect to the central plane in the transverse direction (y/s=1) near the channel exit is also observed.

Flow at x/s=0 requires special attention. The plane x/s=0 in Fig. 8 does not represent the edge of the backstep; it represents the nodal locations nearest to the backstep for the u-velocity component in the grid. Figure 8(a) shows a negative zone for the u-velocity profile in the vicinity of the bottom wall (y/s=0). This zone is associated with the effects of the primary recirculation zone. Similarly, for Re=200 and Re=343 in Figs. 8(b) and 8(c), this zone is more pronounced and the recirculation is also larger as the Reynolds number increases. However, for Re=400 and Re=512, this zone does not start at y/s=0. Hence, a small zone with positive u-component values in the vicinity of the bottom wall is present in Figs. 8(d) and 8(e). For the case of Re=512 the negative u-component zone starts to develop approximately at y/s=0.20. Hence, it can be said that for Re=400 and Re=512 there is a small zone or bubble with positive values for the u-velocity component adjacent to the backstep inside the primary recirculation zone.

Numerical predictions for the transverse v-velocity component at the central plane in the transverse direction (y/s=1) at x/s=0 and x/s=5 are presented in Fig. 9. The plane x/s=0 is located in the vicinity of the backstep whereas the plane x/s=5 is located inside the primary recirculation zone.

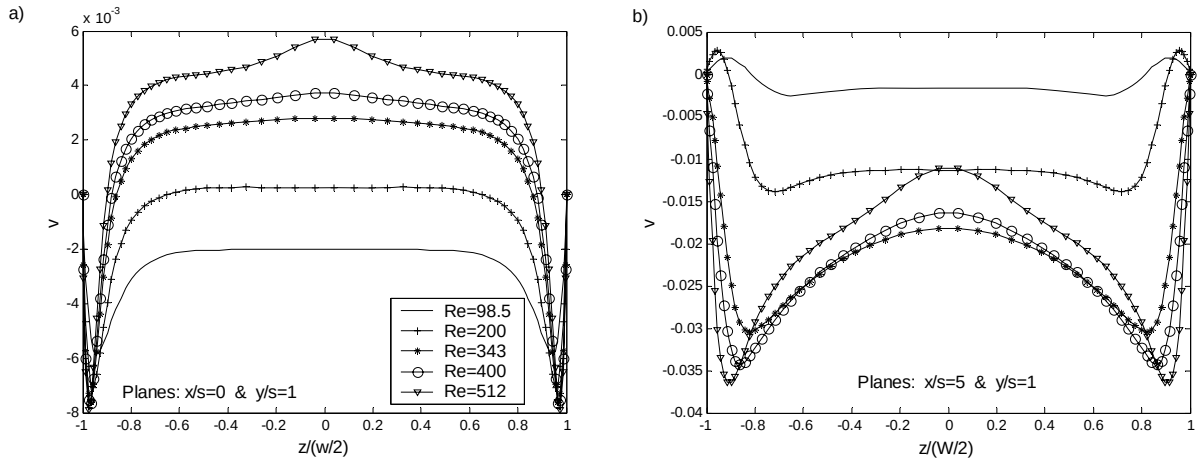

Fig. 9 V velocity component at different x and y planes.

Symmetric behavior with respect to the central plane in the spanwise direction is observed in Figs. 9(a) and 9(b). Figure 9(a) shows that the v-component of the velocity has an order magnitude of 10^{-3} in these planes. In the vicinity of the side walls the transverse component of the velocity presents two peak negative values that can be associated with the minimum in the x_u-line that is developed near the side walls. Figure 9(b) shows that the transverse velocity component in these planes (x/s=5 & y/s=1) has negative values along the spanwise direction. The x-plane that is plotted in this figure lies inside the recirculation zone. Since the values for the v-velocity component are negative in this plane, the flow is directed towards the bottom wall of the channel in this zone.

Figure 10 shows the spanwise w-velocity components at different planes. A plane y/s=0.05 is adjacent to the bottom wall while a plane y/s=1.95 is near the top. The spanwise component of the velocity also presents an inverted symmetric behavior with respect to the central plane in the z-direction. At the central plane in the spanwise direction the w component is equal to zero along the streamwise direction. According to Fig 10(a), the w-component adjacent to the backstep presents negative values in the negative z-coordinate and positive values for the positive z-coordinate. Therefore, in this zone the flow is directed towards the side walls. This could be the reason why the minimum in the x_u-line is located near the side walls and not at the central plane in the z-direction.

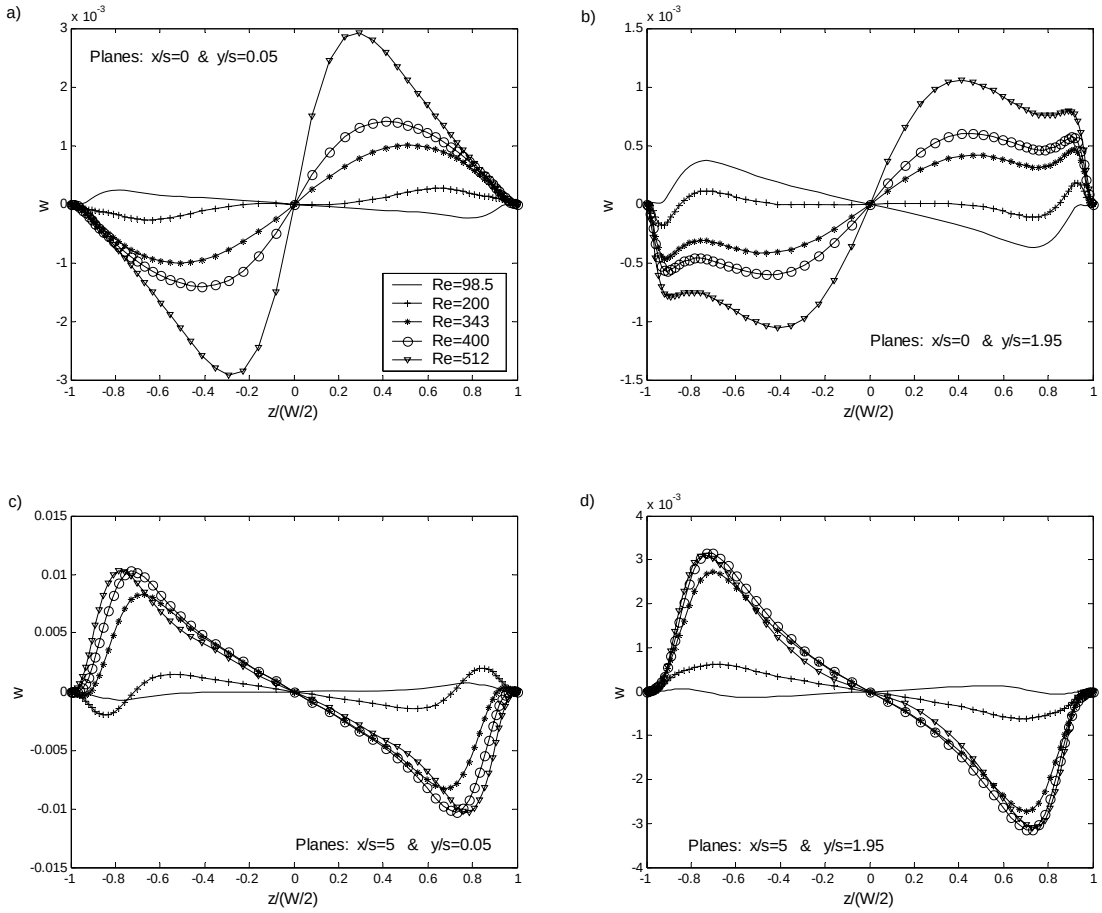

Fig. 10 W velocity components at different planes: a) x/s=0 (step) & y/s=0.05 (bottom), b) x/s=0 (step) & y/s=1.95 (top), c) x/s=5 (reattachment zone) & y/s=0.05 (bottom), d) x/s=5 (reattachment) & y/s=1.95=(top).

As can be seen in the same figure, the spanwise distribution of the w- component remains nearly constant for Re=98.5 but shows strong variation for Re=512. This behavior was also observed for the x_u-line. Hence, it is evident that the primary recirculation zone is influenced by the w-velocity component.

Figure 10(c) shows the situation for a bottom plane inside the recirculation zone. An opposite behavior to the one described for Fig. 10(a) is found in this zone, and the flow is directed towards the central plane z/(w/2)=0. This phenomenon may be the reason for the parabolic profile of the x_u-line in the middle of the channel. The spanwise distribution for the w-velocity component present values close to zero at the central portion of the channel (z/(W/2)=±0.4), this

behavior explains the fact that the x_w-line presents a kind of discontinuity in the central zone of the channel in the spanwise direction (Fig. 5).

Summary

Numerical approximations to solve the convective flow and heat transfer over a three-dimensional backward facing step heated from below at constant heat flux are presented in this work. In the first phase, the code was validated against published experimental data. Our numerical predictions agreed very well with the experimental data.

Reynolds number was varied from Re=98.5 to Re=512. It was found that the x_u-line presents higher variations in the spanwise directions and shifts further downstream as the Reynolds number is increased. Similarly, the spanwise average Nusselt number distributions present higher values at higher Reynolds numbers.

The points of intersection of the x_u-line and the x_w-line are the points where the shear stress along the bottom wall is equal to zero. The intersection point is displaced towards the channel side walls and its position in the spanwise direction is not influenced by the Reynolds number. However, its streamwise location is shifted towards the channel exit as Reynolds number increases. The maximum local Nusselt number along the bottom wall was found to lie in the vicinity of these points.

The velocity profiles reveal that for Reynolds number greater than 343 the flow does not reach fully developed conditions at the channel exit. For all cases considered in this study the flow never reached thermally fully developed flow condition. The spanwise w-component influences the development of the primary reattachment zone adjacent to the backstep.

Nomenclature

AR Aspect ratio, AR=W/s
Cp Specific heat
ER Expansion ratio, ER=2H/s
k Thermal conductivity

L Total length of the channel, L=52s

l Total length of the step, l=2s

Nu Local Nusselt number; $\frac{q_w s}{k\left(T_w - T_0\right)}$

Nu_{avg} Average Nusselt number; $\left[\frac{q_w s}{k\left(\overline{T}_w - T_0\right)}\right]$

p Pressure

Pr Prandtl number

q_w Constant heat flux [Wm^{-2}]

Re Reynolds number; $\frac{2\rho U_0 s}{\mu}$

s Step height

T Temperature

u Velocity component in x direction

U_0 Bulk velocity at the channel inlet

V Vector Velocity field

v Velocity component in y direction

W Channel longitudinal length

w Velocity component in z direction

x, y, z Coordinate directions

Subscripts

0 Inlet conditions

s Solid

w Wall

Greek letters

α Relaxation factors

μ Dynamic viscosity

ρ Density

τ Shear stress at the bottom wall

$\overline{\tau}_{wx}$ Streamwise shear stress component averaged in the spanwise direction $\mu\left(\frac{\overline{du}}{dy}\right)_{y=0}$

References

Armaly B. F., Li, A., Nie, J. H., 2003, "Measurements in three-dimensional laminar separated flow," Int. J. Heat and Mass Transfer, Vol. 46, pp. 3573-3582

Armaly B. F., Li, A., Nie, J. H., 2002, "Three-Dimensional forced convection flow adjacent to backward-facing step," J. of Thermophysics and Heat Transfer, Vol. 16, pp. 222-227

Carrington, D. B., and Pepper, D. W., 2002, "Convective heat transfer downstream of a 3-D backward-facing step," Numerical Heat Transfer, Part A, Vol. 41, pp. 555-578

Chiang, T. P., Sheu, T. W.H., and Tsai, S. F., 1997, "Topological flow structures in backward-facing step channels," Computers and Fluids, Vol. 26, pp. 321-337

Iwai, H., Nakabe, K., Suzuki, K., and Matsubara, K., 2000, "Flow and heat transfer characteristics of backward-facing step laminar flow in a rectangular duct," Int. J. Heat and Mass Transfer, Vol. 43, pp. 457-471

Kakac, S., and Yener, Y., 1995, *Convective Heat Transfer*, 2nd ed., CRC Press, Inc, USA

Nie, J. H., and Armaly, B. F., 2002, "Three-dimensional convective flow adjacent to backward-facing step –effects of step height," Int. J. of Heat and Mass Transfer, Vol. 45, pp. 2431-2438

Nie, J. H., and Armaly, B. F., 2003, "Reattachment of three-dimensional flow adjacent to backward-facing step," Int. J. of Heat Transfer, Vol. 125, pp. 422-428

Patankar, S. V., 1980, *Numerical Heat transfer and Fluid Flow*, Taylor and Francis, USA

Shih, C., and Ho, C. M., 1994, "Three-Dimensional recirculation flow in a backward facing step," J. of Fluids Engineering, Vol. 116, pp. 228-232

Shah, R.K., and London, A.L., 1978, *Laminar flow forced convection in ducts*, Academic Press, New York, USA

ACKNOWLEDGEMENT

Financial support for this work by ANIUS, Mexico is gratefully acknowledged.